The plankton multiplier—positive feedback in the greenhouse

John Woods and Wolfgang Barkmann[1]

Natural Environment Research Council, Polaris House, Swindon SN2 1EU and [1]Oceanography Department, University of Southampton, Southampton, UK

Abstract. The plankton multiplier is a positive feedback mechanism linking the greenhouse effect and biological pump (Woods,J.D., Royal Commission on Environmental Pollution, 1990). As pollution increases the atmospheric concentration of carbon dioxide, the enhanced greenhouse effect induces radiative forcing of the ocean, which diminishes the depth of winter convection, reducing the annual resupply of nutrients to the euphotic zone and therefore the annual primary production. That weakens the biological pump, which contributes to oceanic uptake of CO_2. As the ocean takes up less CO_2, more remains in the atmosphere, accelerating the rise in radiative forcing. We have used a mathematical model of the upper ocean ecosystem, based on the Lagrangian Ensemble method, to estimate the sensitivity of the biological pump to radiative forcing, which lies at the heart of the plankton multiplier. We conclude that increasing radiative forcing by 5 W m^{-2} (equivalent to doubling atmospheric CO_2) reduces the deep flux of particulate carbon by 10%. That sensitivity is sufficient to produce significant positive feedback in the greenhouse. It means that the plankton multiplier will increase the rate of climate change in the 21st century. It also suggests that the plankton multiplier is the mechanism linking the Milankovich effect to the enhanced greenhouse effect that produces global warming at the end of ice ages.

Introduction

The increase in atmospheric carbon dioxide due to burning of fossil fuel is causing global warming by the greenhouse effect (Houghton *et al.*, 1992). The rate of change is reduced by uptake of CO_2 in the ocean. Recent measurements at sea have documented the depletion of ocean mixed-layer CO_2 during the spring plankton bloom (Watson *et al.*, 1991). A significant fraction of the CO_2 consumed by phytoplankton is lost to the deep ocean as detritus (Asper *et al.*, 1992). A global weakening of that biological pump (Volk and Hoffert, 1985) would reduce the net uptake of carbon by the ocean, which is estimated to be 2–3 Gigatonnes year $^{-1}$, about half the rate of atmospheric pollution (Falkowski and Wilson, 1992; Keeling and Shertz, 1992; Sarmiento and Sundquist, 1992). Predictions of climate change due to the greenhouse effect assume that the fraction of CO_2 pollution removed by the ocean will not change as the planet warms (Houghton *et al.*, 1992). That assumption has been questioned. For example, it has been pointed out that global warming will lead to enhanced rainfall and run-off from the continents, reducing mixed-layer salinity in the northern North Atlantic and so inhibiting deep convection in winter (Manabe *et al.*, 1991), which flushes CO_2-enriched water into the deep ocean (a process known as the solubility pump; Volk and Hoffert, 1985). That positive feedback mechanism comes into play after the ocean has been warmed by greenhouse forcing, when enhanced evaporation has made up for the reduction in oceanic IR cooling to the atmosphere. The plankton multiplier mechanism (shown schematically in Figure 1) occurs earlier because it depends not on temperature rise, but on radiative forcing. We have tested that theory by computing the sensitivity of the biological pump to radiative forcing in a one-dimensional
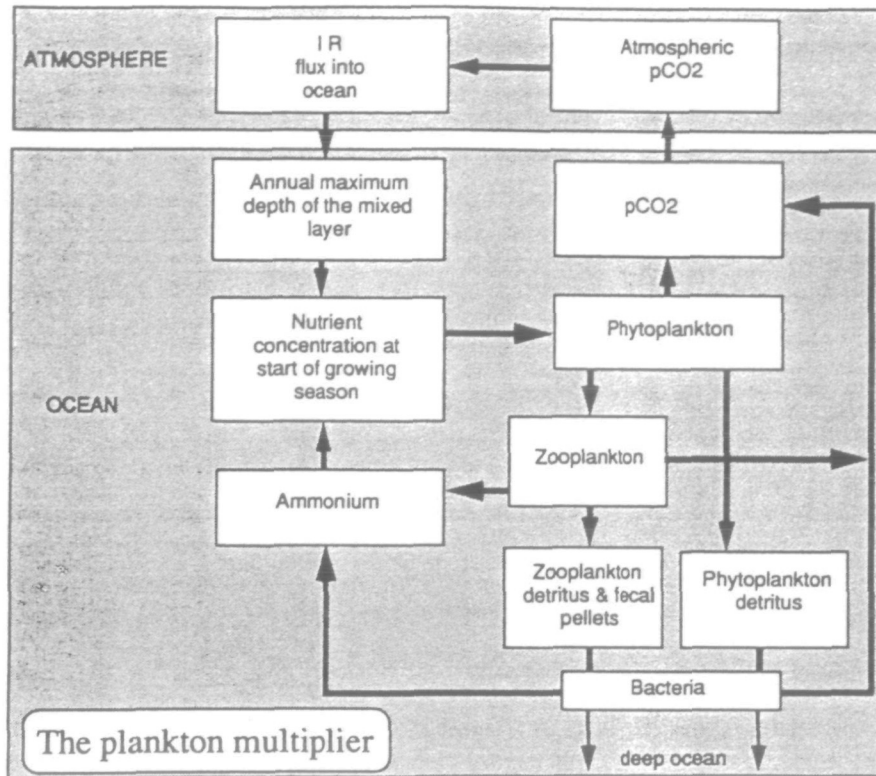
Fig. 1. The plankton multiplier mechanism as represented in our model.

mathematical model of the upper ocean ecosystem [to be documented in detail in Woods (1994)].

The model

Our model (see Appendix) includes equations for processes that change the physical environment (sunlight, turbulence and temperature), the chemical environment (concentrations of nitrate, ammonium and CO_2) and the biological environment (biomasses of phytoplankton, zooplankton and detritus). The ecological equations are similar to those used in Eulerian models of the vertical structure of the upper ocean ecosystem (Fasham *et al.*, 1990), but refined to reveal the subtle changes introduced by greenhouse forcing. The physical environment is described by a Kraus–Turner mixed layer with separate treatment of convective adjustment and turbulent entrainment for more accurate simulation of turbocline response to radiative forcing (Woods and Barkmann, 1986a). Solar radiation is represented by 27 spectral bands of solar radiation; seawater turbidity is controlled by the plankton concentration. The chemical environment has prescribed initial distributions of nitrate (Glover and Brewer, 1988), ammonium and carbon dioxide: nitrate is consumed by photosynthesis, but not regenerated, ammonium (initially zero) is generated by

1054

zooplankton excretion and by microbial action in detritus and faecal pellets. The equations for photosynthesis do not discriminate between nitrate and ammonium. No account is taken of atmospheric input of nitrogen (Owens *et al.*, 1992). Carbon dioxide flows through the sea surface at a rate controlled by the difference between pCO_2 of the atmosphere and ocean mixed layer, calculated using a fixed piston velocity. The model was initialized with mixed-layer pCO_2 equal to 325 p.p.m.v., which gave zero net annual exchange with the atmosphere (345 p.p.m.v.). Carbon dioxide is consumed during photosynthesis and released by zooplankton respiration, excretion and microbial action, in fixed (Redfield) ratio to nitrogen consumption or release. No account is taken of possible effects of CO_2 on phytoplankton growth rate (Richesell *et al.*, 1993). The biological environment comprises varying concentrations of one guild each of phyto-plankton (diatoms) and herbivorous zooplankton (calanoid copepods), plus steady homogeneous concentrations of bacteria and carnivorous zooplankton. The rainout of detritus to the deep ocean comprises dead phytoplankton and zooplankton, and their faecal pellets. That particulate flux is dominated by diatoms which transport carbon in mainly organic form (Cushing, 1992). The change in the partial pressure of dissolved CO_2 was computed using the method of Bacastow and Bjorkstrom (1981) with dissociation constants from Peng *et al.* (1987). The method is similar to that used by Taylor *et al.* (1992), but with constant values of pH = 8.5 and boron concentration.

The interaction between particles (plankton, detritus and faecal pellets) and turbulence in the mixed layer lies at the heart of the plankton multiplier theory and so required particular attention in the model. We used the Lagrangian Ensemble method (Woods and Onken, 1982; Wolf and Woods, 1988) which is uniquely suited to meeting that requirement because it treats the plankton as a cloud of discrete particles and integrates the development of each particle separately along its own individual trajectory. The method permits explicit treatment of plankton locomotion through the unevenly turbulent flow. It also calculates the adaptation of each particle to its changing ambient environment (the ambient environment of a particle is defined as the set of values that the environmental fields have at the particle's location), and its physiological and behavioural response to that adaptation. The equations for particle behaviour are similar to those used by Woods and Barkmann (1993). Phytoplankton particles fall steadily through the water at 1 m day^{-1}, and zooplankton particles migrate diurnally in response to light, food concentration and recent grazing success. Dead plankton and faecal pellets were treated explicitly as particles sinking at 1 m day^{-1}; the model simulates microbial extraction of each particle's nitrogen and carbon, and their release to the seawater as ammonium and carbon dioxide.

Integration

To test the plankton multiplier hypothesis, we integrated the model for 10 years in half-hour time steps, under the influence of surface fluxes of solar and thermal radiation, latent and sensible heat, and CO_2, starting from a prescribed initial state. The model was forced by Bunker's monthly climatology (Isemer and

1055

Hasse, 1987) and solar elevation interpolated to half-hourly values at a fixed location in the northeast Atlantic (40°N, 27°W). Haney (1971) flux correction was used to reduce excessive summer temperature rise in the mixed layer when greenhouse forcing was added. No correction was made for advection: water moves slowly at the chosen site (Woods, 1987) and the relative displacements at different depths in the water column by eddies and Ekman transport (both <100 km year^{-1}) do not introduce substantial changes in the water column in
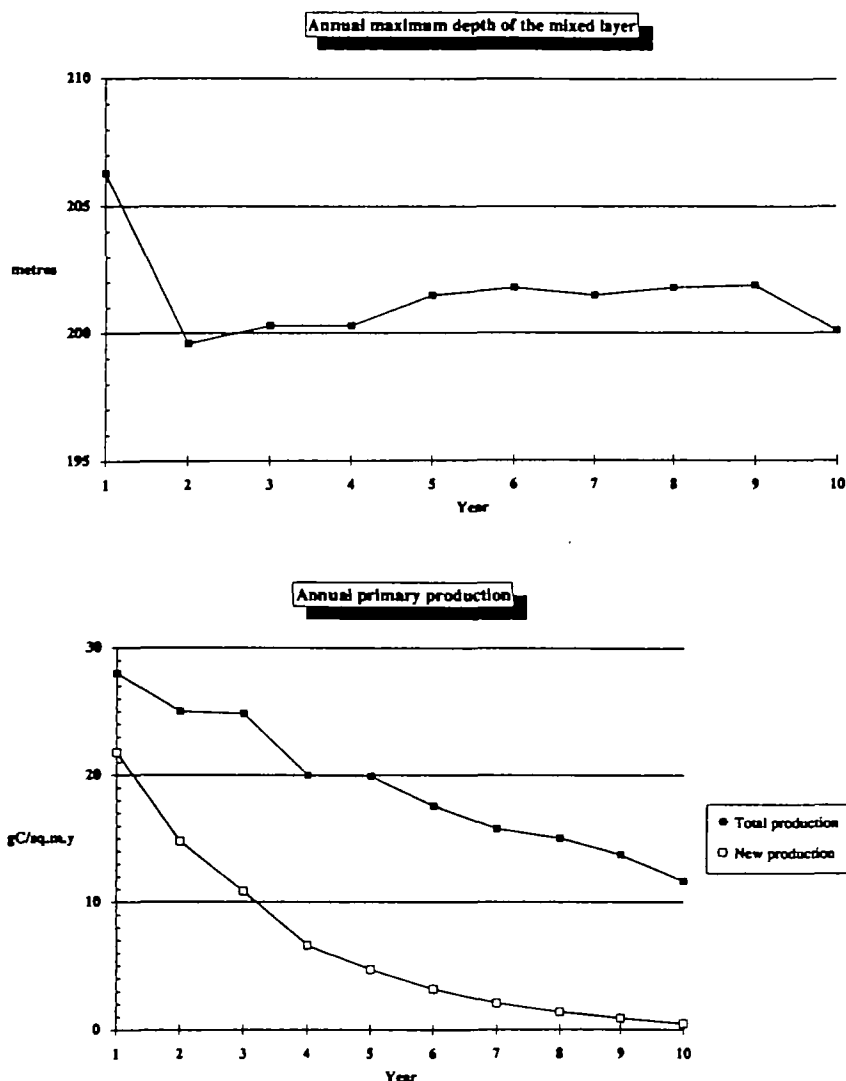

Fig. 2. The control integration. (a) Annual maximum depth of the mixed layer. (b) Annual primary production. (c) Mixed-layer nitrogen concentration at the start of each growing season. (d) Scaled annual production, grazing (×2.28) and flux of detritus (×9).

this region of weak horizontal environmental gradients. Ekman pumping (30 m year^{-1}) was also neglected.

Simulation without greenhouse forcing

The first numerical experiment simulated the response of the ecosystem to the regular annual cycle of forcing without greenhouse forcing. The results of this control run are illustrated in Figures 2 and 3. The euphotic zone occupies the upper portion of the seasonal boundary layer, which extends down to the annual maximum depth of the mixed layer (D). Figure 2a shows that the initial depth (206.3 m) taken from climatology (Robinson *et al.*, 1979) was a few metres deeper than the model diagnosed from the prescribed Bunker climatology and
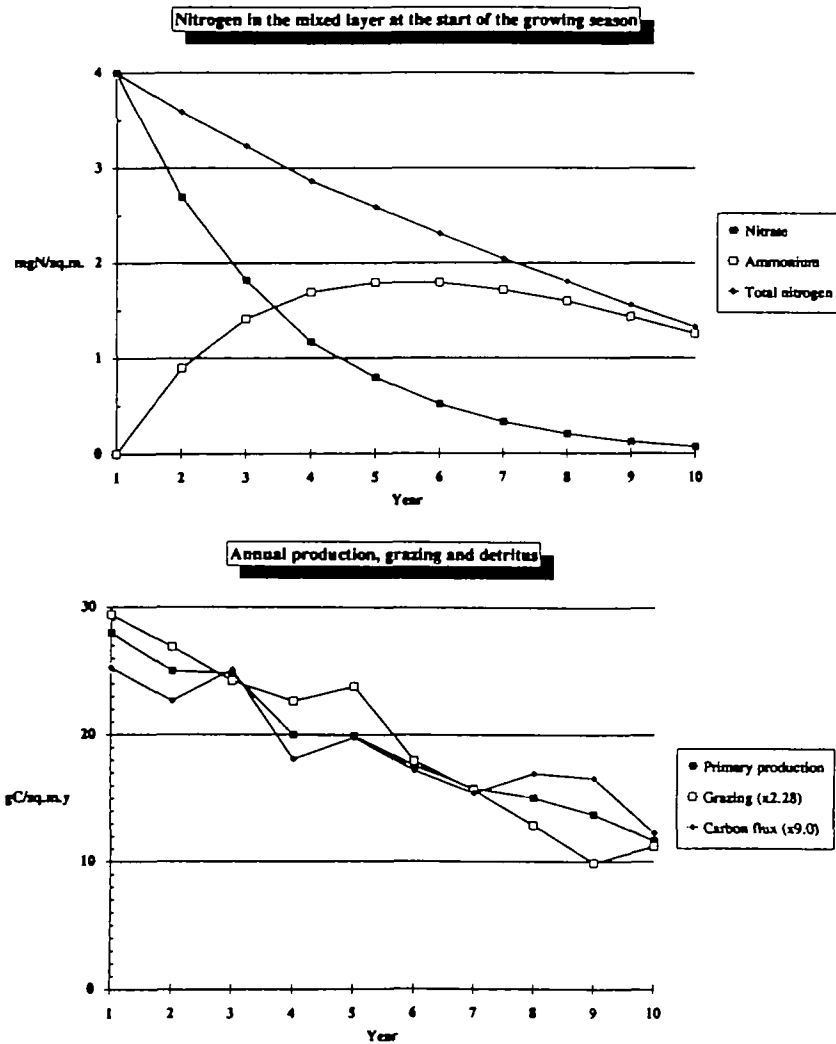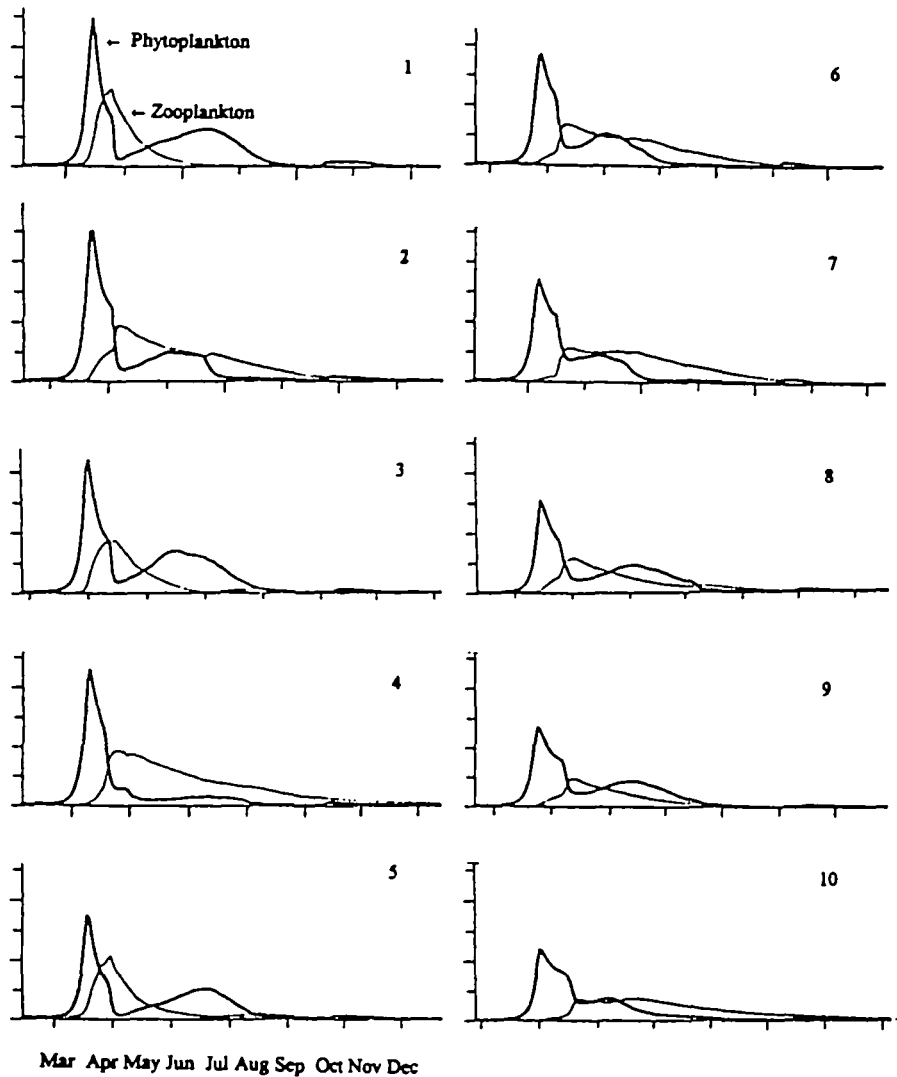

Fig. 2. Continued.

Fig. 3. Variation of phytoplankton and zooplankton biomasses during each of the 10 years. (Tick marks: biomass 25 mmol N m^{-2}; time 50 days.)

the phytoplankton biomass which controls seawater turbidity, and therefore the depth of solar heating (Woods *et al.*, 1984); variation in biomass changed D by 1% (199.6–201.9 m). The annual primary production (Figure 2b) fell by 40% (28 to 17 g m^{-2} year^{-1}) over the 10 years of integration, as the total nitrogen supply was depleted by fallout of particles from the seasonal boundary layer into the permanent thermocline. The decrease in new production (that attributed to consumption of nitrate) fell by 95% (from 22 to 1 g C m^{-2} year^{-1}). The changes in nitrogen supply are shown in Figure 2c: the ammonium rises to a maximum in

year five and declines thereafter. Nutrient availability is the dominant factor influencing inter-annual change in the ecosystem. The progressive depletion of nutrients and the decline in primary production is similar to that occurring in a water column circulating slowly around the eastern side of the gyre as it makes the transition from seasonal to permanent oligotrophy after entering the zone of net annual heating (Woods, 1985; Woods and Barkmann, 1986b).

Each year CO_2 flows into the ocean during the spring bloom, when photosynthesis depletes the concentration in the mixed layer, then flows out when summer heating raises the partial pressure above that of the atmosphere; inflow returns as the mixed layer cools in winter. The net annual inflow of CO_2 compensates for (i) the loss of carbon in particles sinking into the permanent thermocline, and (ii) the decreasing carrying capacity of the water column warmed by greenhouse forcing (Figure 5).

There is evidence of inter-annual variability superimposed on the smooth trends in production and nutrient concentration. Note, for example, the relatively high value of primary production in year 3, followed by a sharp decrease in year 4, which modulates the annual maximum depth of the mixed layer. This inter-annual variability is an example of the natural chaos found in all such models of predator–prey interaction (May, 1981; Scheffer, 1991). The effect is clearly seen in the time series of phytoplankton and zooplankton biomass for each year (Figure 3).

The properties of this chaotic variability will be the subject of another publication. Here we shall consider whether it is sensitive to greenhouse forcing, and therefore a significant factor in the plankton multiplier. To do so, it is convenient to concentrate on a single variable, grazing efficiency, which lies at the heart of inter-annual variability. Figure 2d shows the inter-annual modulation of primary production, grazing and the flux of carbon carried by detritus into the permanent thermocline. Note the inverse correlation between grazing and deep carbon flux. They have an inter-annual variation of ~10% of the annual mean values; about twice that in primary production.

To summarize, the model simulates the development of the ecosystem over 10 years with sufficient precision to resolve changes of a few centimetres in the annual maximum depth of the mixed layer caused by inter-annual variation in phytoplankton biomass. The progressive loss of nitrate from the seasonal boundary layer and the corresponding decline in new production has a 2 year half-life. Total primary production is sustained by ammonium generated by zooplankton excretion and remineralization of detritus in the seasonal boundary layer; it halves (approximately linearly) in 8 years. Net CO_2 flow into the ocean compensates each year for the loss of carbon from the seasonal boundary layer due to particles sinking into the permanent thermocline. Non-linear interactions between primary and secondary production modulate them significantly within each year, and produce 10% variation in grazing. That produces a corresponding (inverse) modulation of the flux of particulate carbon and nitrogen into the permanent thermocline. The model is capable of simulating the essential ingredients of the biological pump with precision sufficient for testing the plankton multiplier hypothesis.

1059

The response to greenhouse forcing

The next set of integrations of our model were designed to reveal the sensitivity of the biological pump to changes in surface radiative forcing. Greenhouse forcing is reducing the IR cooling of the ocean by 1 W m^{-2} every 10 years. Will that alter oceanic uptake of CO_2 by the time atmospheric concentration doubles in ~50 years? In order to address that question, we integrated our model with the same conditions as those described above (the control run) apart from surface IR flux reducing at 1, 2 or 3 W m^{-2} per year respectively. The shortened time scale was adopted to ensure that changes induced by radiative forcing would be clearly distinguishable from grazing noise within 10 years, i.e. before new production became negligible and the water column was half-way to permanent oligotrophy.

Table I shows how the sea surface (mixed layer) temperature at the end of each winter rises year by year as heat accumulates in the ocean in response to the imposed radiative forcing. As its temperature rises, the ocean transfers more heat to the atmosphere each year, but that increase is smaller than the imposed reduction in IR cooling. Table I shows the net change in annual heat flow through the ocean surface simulated in our model by the Haney flux correction term. Consider the integration with radiative forcing of 3 W m^{-2} per year. In year 10, the forcing has risen to 30 W m^{-2}, but the net heat flux through the surface is only 2.01 W m^{-2} greater than in the control run, because the winter surface temperature has risen by 0.8 K. Thus, the model simulates the essential phenomenon of global warming due to the greenhouse effect: increasing concentration of greenhouse gases reduces IR cooling of the ocean, which then accumulates heat, becomes warmer and increases heat flow to the atmosphere mainly by evaporation, and to a lesser extent by sensible heat and thermal radiation. The greenhouse mechanism trades IR cooling of the ocean for evaporation with profound consequences for the climate of the atmosphere.

The net decrease in heat flux through the surface leads to significant changes in the annual maximum depth of the mixed layer, which occurs each year at the end of the winter cooling season (Figure 4a). The sensitivity to radiative forcing was 4.5 m W^{-1} m^{-2} in the first year, while nitrate is still plentiful and primary production still high. The winter mixed layer continues to get shallower as radiative forcing increases, but it responds to the net annual heat flux, which (Table I) is less than the IR forcing. Superimposed on the trend, there are inter-annual variations in the winter mixed-layer depth, which are larger than the inter-annual trend. They are caused by inter-annual variation in the sea surface temperature in summer, due to year-to-year differences in phytoplankton biomass due to grazing (Figure 3), so care is needed in diagnosing the model results. Happily, the curves in Figure 4a for different forcing rates do not overlap throughout the 10 year integrations. By the tenth year, when IR forcing has reached 10, 20 or 30 W m^{-2}, respectively, in the three integrations, the annual net heat flux deficits are 0.96, 1.81 and 2.31 W m^{-2}, respectively, and the annual maximum depth of the mixed layer is shallower than the control by 13.9, 21.1 and 28.9 m, respectively. In round terms, over 10 years integration, the

1060

Table I. Annual net surface heat fluxes and minimum mixed-layer temperatures

Year	Control run	Qnet [W m^{-2}]			Control run	SST [C]		
	W m^{-2} year^{-1}	1 W m^{-2} year^{-1}	2 W m^{-2} year^{-1}	3 W m^{-2} year^{-1}		1 W m^{-2} year^{-1}	2 W m^{-2} year^{-1}	3 W m^{-2} year^{-1}
1	1.37	1.62	1.77	2.15	15.02	15.02	15.02	15.03
2	1.37	1.73	2.30	2.93	15.10	15.11	15.12	15.14
3	1.37	2.12	2.93	3.49	15.17	15.19	15.23	15.28
4	1.37	2.07	2.77	3.38	15.24	15.30	15.37	15.44
5	1.37	1.84	2.59	3.31	15.31	15.40	15.50	15.61
6	1.37	2.18	3.30	3.82	15.38	15.49	15.63	15.77
7	1.37	2.29	2.87	3.53	15.46	15.60	15.78	15.95
8	1.37	2.08	2.87	3.67	15.53	15.71	15.92	16.12
9	1.37	2.51	2.79	3.93	15.61	15.81	16.06	16.29
10	1.37	2.33	3.18	3.68	15.68	15.93	16.20	16.48

Annual maximum depth of the mixed layer
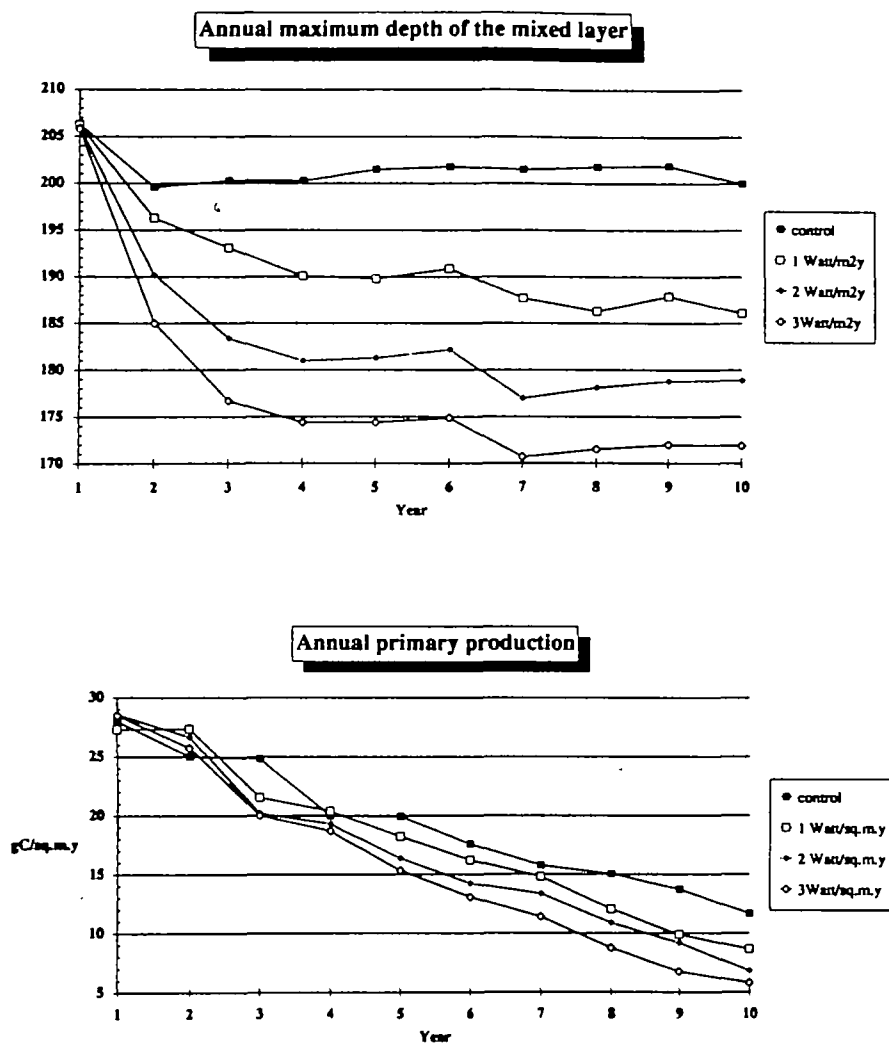

Annual primary production

Fig. 4. Impact of radiative forcing on the ecosystem. (a) Annual maximum depth of the mixed layer. (b) Primary production. (c) Carbon in detritus accumulating in the permanent thermocline. (d) Grazing efficiency.

sensitivity of the mixed depth at the start of the heating season to imposed forcing is 1 m shallower per $W\ m^{-2}$; it is an order of magnitude more sensitive to changes in the net surface heat flux.

The mixed layer becomes depleted in nitrogen during the growing season and is recharged in winter when it entrains nutrient-rich water from deeper in the seasonal boundary layer. The nitrogen concentration at the start of each growing season depends on the annual maximum depth of the mixed layer (D). As D is reduced by radiative forcing, the winter nutrient concentration declines and so in consequence does the primary production. Superimposed on that decline is the
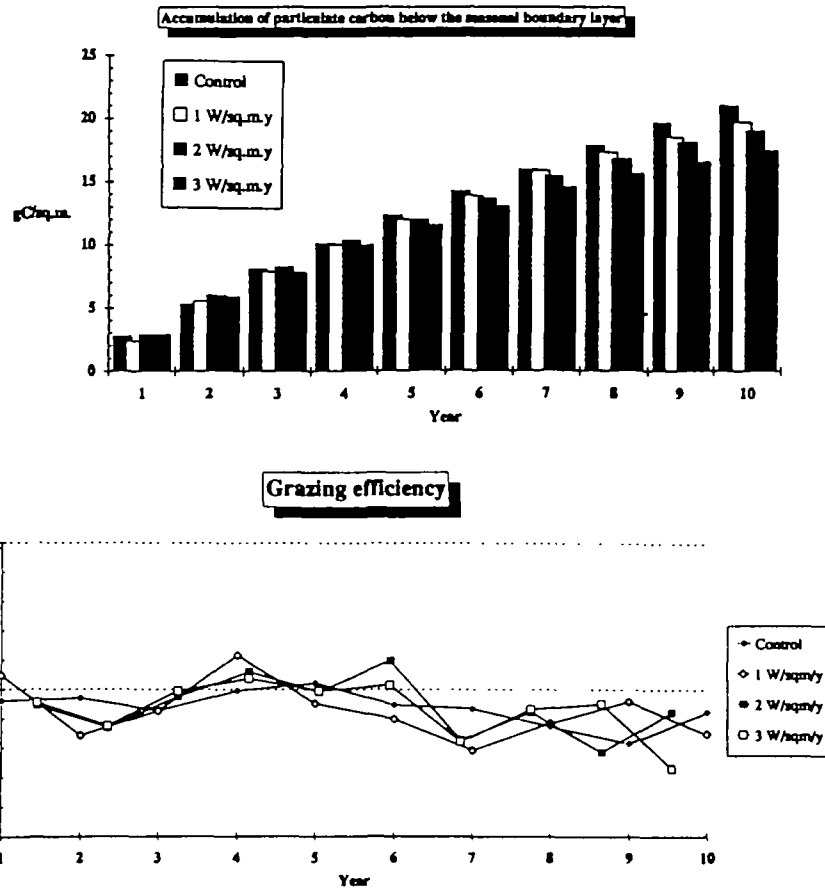
1062

Fig. 4. Continued.

usual modulation by grazing noise, but the curves in Figure 4b show a monotonic decrease in primary production with radiative forcing, with a mean response (in year 10) of 2.4 g C m^{-2} year^{-1} per 10 W m^{-2}, which is 21% of the production in the control run that year. This decrease in primary production is matched by a reduction in loss of carbon from the seasonal boundary layer by detritus (note the changes in the last 5 years of Figure 4c) and by influx of CO_2 from the atmosphere (Figure 5). There is no evidence that grazing efficiency responds to radiative forcing (Figure 4d).

To summarize, the biological pump is sensitive to greenhouse forcing. The deep carbon flux is reduced by ~10% when the IR forcing reaches 5 W m^{-2}, equivalent to a doubling of atmospheric CO_2. The response is due to a reduction of 5.7 m in the depth (D) of the seasonal boundary layer, which diminishes the supply of nitrogen to the euphotic zone. The change in mixed-layer depth is coupled to that of primary production. There is no evidence that grazing efficiency or its variability respond to greenhouse forcing.
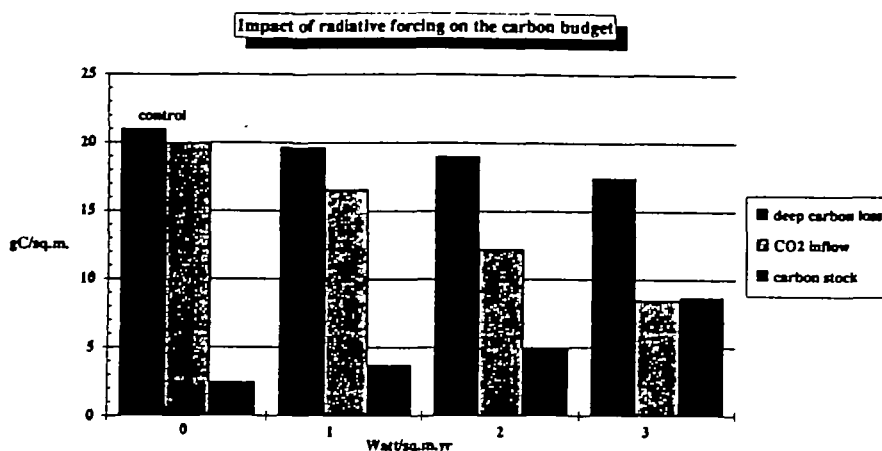
1063

Fig. 5. The influence of radiative forcing on the carbon budget over 10 years. The influx of CO_2 balances the loss of carbon to the deep ocean and the decreasing carrying capacity of the seasonal boundary layer as it gets warmer and shallower.

As a check, we performed another set of 10-year integrations with fixed IR deficits of 5, 10, 12.5 or 15 W m^{-2}. The sensitivity of the biological pump was the same as in the transient forcing runs, within the uncertainty set by grazing noise.

Feedback in the greenhouse

The model results show that by the time atmospheric CO_2 has doubled, the associated radiative forcing of the ocean will have reduced the biological pump by some 10%. That is the strength of the plankton multiplier, which depends on the fractional change in the annual maximum depth of the mixed layer. Existing general circulation models do not have the precision to determine that sensitivity; it might be estimated geographically by Lagrangian integration of our model at a variety of sites using the method of Woods and Barkmann (1986b), but that will be the subject of another publication. Here it suffices to note that the plankton multiplier mechanism works everywhere that nocturnal convection controls D. Our investigation addressed changes occurring in the ventilation regime of the gyre, but the impact of reducing D will have the same sign in the entrainment regime (see Woods, 1985): the supply of nutrients to the euphotic zone will diminish there, too. The only region where it does not work is in about half of the tropics where D is controlled not by nocturnal convection, but by Ekman currents. However, the biological pump is weak in that permanently oligotrophic region of low primary production which does not contribute significantly to the control of atmospheric CO_2 (Wenk and Seigenthaler, 1985), so the results of our sensitivity study are valid globally. The plankton multiplier gives positive feedback everywhere and, therefore, a net global positive feedback to the greenhouse effect.

The reduction in annual maximum depth of the mixed layer as radiative forcing increases will also weaken the solubility pump, in which CO_2 dissolved in

1064

the seasonal boundary layer is ventilated into the permanent thermocline (Woods, 1985). Ventilation decreased as greenhouse forcing strengthened during the last deglaciation (Slowey and Curry, 1992).

Finally, we note that the sensitivity of the annual maximum depth of the mixed layer to radiative forcing does not depend on the radiation being thermal: it is the same for changes in solar radiation. A decrease in climatological mean cloud cover (Ramanathan and Collins, 1991; Fu *et al.*, 1992) is just as effective in reducing the annual maximum depth of the mixed layer and thereby weakening the biological pump.

On a longer time scale, cyclic variation in the Earth's orbit leads to redistribution of annual mean solar heating across the globe, with local amplitude of a few W m^{-2}. The ice age cycle is linked to this Milankovich effect by a mechanism in which the slowly changing radiative forcing provoked a greenhouse effect that doubled the atmospheric concentration of CO_2 in 10 000 years as the Earth emerged from the last glaciation (Berger *et al.*, 1984). At the same time, the atmospheric concentration of methyl sulphonic acid (MSA) decreased, suggesting that the greenhouse effect was provoked by a reduction in oceanic primary production, phytoplankton being the source of MSA (Andrae, 1992). We suggest that the plankton multiplier mechanism may have been responsible for that decline. This explanation for global warming at the end of the last ice age has the advantage that it links radiative forcing by the Milankovich effect directly to global warming by the greenhouse effect. It avoids the need to assume that the feeble Milankovich forcing triggers the greenhouse effect by first warming the ocean.

References

Andrae,M.O. (1992) The global biogeochemical sulphur cycle. In Moore,B.,III and Schimel,D. (eds), *Trace Gases and the Biosphere*. UCAU/Office for Interdisciplinary Earth Studies, Boulder, CO, pp. 87–128.

Asper,V.L., Deuser,W.G., Knauer,G.A. and Lohreny,S.E. (1992) Rapid coupling of sinking particle fluxes between surface and deep ocean waters. *Nature*, 357, 670–672.

Bacastrow,R. and Bjorkstrom,A. (1981) Comparisons of ocean models for the carbon cycle. In Bolin,B. (ed.), *Carbon Cycle Modelling*. Wiley, New York, pp. 29–79.

Berger,A., Imbrie,J., Hays,G., Kukla,G. *et al.* (eds) (1984) *Milankovich and Climate*. Reidel, Dordrecht.

Cushing,D.H. (1992) The loss of diatoms in the spring bloom. *Phil. Trans. B.*, 335, 237–246.

Falkowski,P.G. and Wilson,C. (1992) Phytoplankton productivity in the North Pacific ocean since 1900 and implications for absorption of anthropogenic CO_2. *Nature*, 358, 741–743.

Fasham,M.J.R., Ducklow,H.W. and McKelvie,S.M. (1990) A nitrogen-based model of plankton dynamics in the oceanic mixed layer. *J. Mar. Res.*, 48, 591–639.

Fu,R., del Genio,A.D., Rossow,W.B. and Liu,W.T. (1992) Cirrus-cloud themostat sea surface temperatures tested using satellite data. *Nature*, 358, 394–397.

Glover,D.M. and Brewer,P.G. (1988) Estimates of wintertime mixed layer nutrient concentrations in the North Atlantic. *Deep-Sea Res.*, 35, 1525–1546.

Haney,R.L. (1971) Surface thermal boundary conditions for ocean circulation models. *J. Phys. Oceanogr.*, 1, 241–248.

Houghton,J.T., Callandar,B.A. and Varney,S.K. (1992) *Climate Change 1992*. Cambridge University Press, Cambridge.

Isemer,H.J. and Hasse,L. (1987) *The Bunker Climate Atlas of the North Atlantic Ocean*. Springer-Verlag, Berlin.

1065

Keeling,R.F. and Shertz,S.R. (1992) Seasonal and interannual variations in atmospheric oxygen and implications for the global carbon cycle. *Nature*, 358, 723–727.

Manabe,S., Stouffer,R.J., Spelman,M.J. and Bryan,K. (1991) Transient response of a coupled ocean–atmosphere model to gradual changes of atmospheric CO_2. Part 1: Annual mean response. *J. Climate*, 4, 785–818.

May,R. (ed.) (1981) *Theoretical Ecology*. Blackwell, Oxford.

Owens,N.J.P., Galloway,J.N. and Duce,R.A. (1992) Episodic atmospheric nitrogen deposition to oligotrophic oceans. *Nature*, 357, 397–399.

Peng,T,-H., Takahashi,T., Broecker,W.S. and Olafsson,J. (1987) Seasonal variability of carbon dioxide, nutrients and oxygen in the northern North Atlantic surface water: observations and a model. *Tellus*, B39, 439–458.

Ramanathan,V. and Collins,W. (1991) Thermodynamic regulation of ocean warming by cirrus clouds deduced from observations of the 1987 El Niño. *Nature*, 351, 27–32.

Richessel,U., Wolf-Gladrow,D.A. and Smetacek,V. (1993) Carbon dioxide limitation of marine phytoplankton growth rates. *Nature*, 361, 249–251.

Robinson,M.K.R., Bauer,A. and Schroeder,E.H. (1979) *Atlas of North Atlantic–Indian Ocean Monthly Mean Temperature and Mean Salinities of the Surface Layer*. Department of the Navy, Washington, DC.

Sarmineto,J.L. and Sundquist,E.T. (1992) Revised budget for the oceanic uptake of anthropogenic carbon dioxide. *Nature*, 356, 589–593.

Scheffer,M. (1991) Should we expect strange attractors behind plankton dynamics—and if so, should we bother? *J. Plankton Res.*, 13, 1291–1305.

Slowey,N.C. and Curry,W.B. (1992) Enhanced ventilation of the North Atlantic gyre thermocline during the last glaciation. *Nature*, 358, 665–668.

Taylor,A.H., Watson,A.J. and Robertson,J.E. (1992) The influence of the spring phytoplankton bloom on carbon dioxide and oxygen concentrations in the surface waters of the northeast Atlantic during 1989. *Deep-Sea Res.*, 39, 137–152.

Volk,T. and Hoffert,M.I. (1985) Ocean carbon pumps: analysis of relative strengths and efficiencies in ocean-driven CO_2 changes. In Sundquist,E.T. and Broecker,W.S. (eds), *The Carbon Cycle and Atmospheric CO_2: Natural Variations, Archæan to Present*. American Geophysical Union, Washington, DC, 32, pp. 99–110.

Watson,A.J., Upstill-Goddard,R.C. and Liss,P.S. (1991) Air–sea gas exchange in rough and stormy seas measured by dual-tracer technique. *Nature*, 349, 145–147.

Wenk,T. and Siegenthaler,U. (1985) The high-latitude oceans as a control of atmospheric CO_2. In Sundquist,E.T. and Broecker,W.S. (eds), *The Carbon Cycle and Atmospheric CO_2: Natural Variations, Archæan to Present*. American Geophysical Society, Washington, DC, 32, pp. 185–194.

Wolf,K.U. and Woods,J.D. (1988) Lagrangian simulation of primary production in the physical environment—the deep chlorophyll maximum. In Rothschild,B.J. (ed.), *Towards a Theory of Biological–Physical Interactions in the World Ocean*. Kluwer, Dordrecht, pp. 51–70.

Woods,J.D. (1985) Physics of thermocline ventilation. In Nihoul,J.C.J. (ed.), *Coupled Ocean–Atmospheric Models*. Elsevier, Amsterdam.

Woods,J.D. (1987) The warm water sphere of the Northeast Atlantic. Institut für Meereskunde an der Universität Kiel.

Woods,J.D. (1990) The plankton multiplier. Royal Commission on Environmental Pollution.

Woods,J.D. (1993) Plankton ecology modelling by the Lagrangian Ensemble method. *Adv. Mar. Biol.*, in preparation.

Woods,J.D. and Barkmann,W. (1986a) The influence of solar heating on the upper ocean I The mixed layer. *Q. J. R. Meteorol. Soc.*, 112, 1–27.

Woods,J.D. and Barkmann, W. (1986b) A Lagrangian mixed layer model of 18° water formation in the Sargasso Sea. *Nature*, 319, 574–576.

Woods,J.D. and Barkmann,W. (1993) Diatom demography in winter—simulated by the Lagrangian Ensemble method. *Fisheries Oceanogr.* (in press).

Woods,J.D. and Onken,R. (1982) Diurnal variation and primary production in the ocean—preliminary results of a Lagrangian ensemble model. *J. Plankton Res.*, 4, 735–756.

Woods,J.D., Barkmann,W. and Horch,A. (1984) Solar heating of the world ocean. *Q. J. R. Meteorol. Soc.*, 110, 633–656.

Appendix

The one-dimensional ecology model includes a phytoplankton model, which is based on a quota method for growth and reproduction, a model of vertical migration and growth of herbivorous zooplankton, a carbon model and a physical upper ocean mixed-layer model forced by surface buoyancy fluxes. Section 1 describes the equations and parameters used in the biological model. In section 2, the equations used in the carbon model are presented.

(1) The biological model

Phytoplankton

(a) Cells

The variables of state for each phytoplankton cell are:

(1) depth: z
(2) light adaptation: I_m
(3) internal nitrogen pool: N_p
(4) internal energy pool: E_p

Phytoplankton growth depends on the change in nutrients and energy in each plant. The governing equations are as follows.

(i) Uptake of nitrate $N(z)$ and ammonium $A(z)$

$$\frac{\partial N_p}{\partial t} = U_{max} \frac{N(z)}{N(z) + k_N} + u_{max} \frac{A(z)}{A(z) + k_A}$$

$$U_{max} = u_{max} = 4 \times 10^{-10} \text{ mmol N h}^{-1} \qquad k_N = k_A = 0.5 \text{ mmol m}^{-3}$$

(ii) Photosynthesis and light adaptation

$$\frac{\partial E_p}{\partial t} = E_{abs} - R_p$$

$$E_{abs} = k_F A I(z) e^{-I/I_m}, \qquad \frac{\partial I_m}{\partial t} = \frac{I(z) - I_m}{t_a}$$

where A = plankton cross-section area πr^2, radius r = 10 μm, irradiance = $I(z)$, phytoplankton adaptation time $t_a = 5^h$ and absorption parameter $k_F = 0.63$.

(iii) Respiration

$$R_p = k_p \frac{B}{B + k_r} W(T)$$

1067

$$W(T) = 0.3 + 0.7T/T_r$$

where the respiration parameter $k_p = 0.2\ \mu J\ h^{-1}$.

The phytoplankton cells are randomly distributed within the mixed layer. A sinking velocity of 1 m day^{-1} is applied in the diurnal and seasonal thermocline.

(b) Particle

In the Lagrangian Ensemble method, the cells are bundled into particles which move through the water like individual plankters. Every organism in a particle has the same adaptive state. The number of organisms per particle is modified by reproduction, mortality and grazing.

Variable of state:

number of cells: n_p

(i) Reproduction

Reproduction (cell division) occurs when the energy and nutrient pools both exceed their respective values (E_c, N_c). The number of cells is doubled and half the excess energy and nitrogen is transferred to the internal pools of the new cells.

$$\Delta n_p = n_p[1 - N_c\delta(N_p)][1 - E_c\delta(E_p)]$$

where

$$\delta(a) = \lim_{b \to 0} F(a,b): \cdot$$

$$F(a,b) = \frac{1}{b} \text{ for } 0 < a < b \text{ else } F(a,b) = 0$$

and $a = N_p$, $b = N_c$.

$$N_{p(new)} = 0.5(N_{p(old)} - N_c),\ E_{p(new)} = 0.5(E_{p(old)} - E_c)$$

$$E_c = 0.14\ mJ \qquad N_c = 4\ pmol\ N$$

(ii) Mortality

Phytoplankton mortality depends on the change in the energy pool due to respiration. A steadily sinking cell loses energy until the energy pool is empty. A this stage, the organism is declared to be dead and will be treated as detritus.

$$\Delta n_p = -E_{min}n_p\delta(E_p)$$

(iii) Grazing

The amount of phytoplankton biomass reduced by grazing in each 1 m depth

1068

interval is recalculated into the equivalent number of cells. Then the organisms in each particle within the 1 m depth interval are reduced by the corresponding percentage of the lost biomass.

$$\frac{\partial n_p}{\partial t} = -n_p \frac{\Sigma l_g}{P(z)}$$

where Σl_g represents the phytoplankton biomass loss and $P(z)$ is the phytoplankton biomass per depth interval.

Herbivorous zooplankton

(a) Individuals

The variables of state for each herbivore are:

(1) depth: z
(2) state of satiation: S
(3) weight: G
(4) age: A

Zooplankton growth and reproduction depend on the ingestion of phytoplankton biomass. The vertical migration is controlled by the visible light and the food supply. The governing equations are:

(i) Ingestion

$$I_g = \frac{W(T,G)}{|z_2 - z_1|} \int_{z_1}^{z_2} FP^*(z) \frac{P^*(z)}{P^*(z) + k_I}\, dz$$

$$|z_2 - z_1| = |V_m| dt$$

V_m: vertical migration velocity

$$P^*(z) = P(z) - P_m, \qquad 0 < I_g < I_{gmax}$$

$$W(T,G) = \left[0.3 + 0.7 \frac{T(z)}{T_r}\right] \frac{G_{eff}^{0.7}}{G_{max}^{0.7}}$$

$$I_{gmax} = 4.2 \text{ cells s}^{-1} - 3.2 \text{ cells s}^{-1} S(t)$$

filtration rate $F = 0.3 \times 10^{-9} \text{ m}^3 \text{ s}^{-1}$
$P(z) =$ phytoplankton concentration [cells m^{-3}]
minimum concentration for grazing $P_m = 10^5$ cells m^{-3}
half-saturation parameter $k_I = 4.0 \times 10^6$ cells m^{-3}.

(ii) Growth

$$\frac{\partial G}{\partial t} = k_a I_g c - R_s k_a I_g c - R_b G_{max}^{0.7}[W(T,G) + k_p]$$

I_g: ingestion k_a: assimilation rate

c = carbon content of one phytoplankton cell (460 pg C)

Metabolic respiration rates:

(a) rate proportional to the food assimilated: $R_s k_a I_g$
(b) basal rate: $R_b W(T,G) G_{max}^{0.7}$

$R_b = 0.3 \times 10^{-3} \, h^{-1}$

$$k_a (1 - R_s) = 0.7$$

$0.3 c I_g$ represents the faecal pellet biomass.

'background' respiration: $R_b k_b G_{max}^{0.7}$, $k_b = 0.1$
maximum weight $G_{max} = 10 \, \mu g \, C$
effective weight $G_{eff} \leq G_{max}$
reference temperature $T_r = 10°C$
   When the total respiration exceeds the actual weight G, the animal is declared dead.

(iii) Vertical migration

$$V_m = k_v V_{max} W(T,G)$$

maximum speed V_m: 45 m day^{-1}

$$k_v = MIN[k, sign(1,k)]; \qquad for \, I_0 = 0 \, and \, \frac{\partial S}{\partial t} < 0: k_v = -k_v$$

$$k = 0.4[I(z) - I_r (2 - S)],$$
$$sign:a,b) = |a| \, for \, b \geq 0, \, or \, -|a| \, for \, b < 0$$

reference radiation I_r: 1 W m^{-2}

I_0: surface irradiance

Thermocline migration:

During the daytime, the herbivores follow a target isolume $I_r(2 - S)$:

1070

(a) $I(z) > I_r(2 - S)$: $k_v > 0 \rightarrow V_m$ positive (downward motion)

(b) $I(z) < I_r(2 - S)$: $k_v < 0 \rightarrow V_m$ negative (upward motion)

At night, the vertical migration is controlled by the rate of change of satiation:

(a) $\dfrac{\partial S}{\partial t} \geq 0$: $k_v < 0 \rightarrow V_m$ negative

(b) $\dfrac{\partial S}{\partial t} \geq 0$: $k_v < 0 \rightarrow V_m$ positive

Mixed layer:

The zooplankters are randomly distributed within the mixed layer. During the daytime, the additional vertical displacememnt $V_m \, \delta t$ is added.

(iv) Satiation

$$\frac{\partial S}{\partial t} = \frac{1}{t_m} \left[\frac{I_g}{I_{gmax}} - S \right]$$

relaxation time $t_m = 4$ h

(b) Particle

The number of individual plankters per particle is modified by reproduction, predation and by starvation. The reproduction takes place 20 days after the animals have reached their maximum weight. After the eggs are hatched, the numbers of adults decrease over the next 20 days. The transition from a juvenile to an adult zooplankter takes place when G_{max} is exceeded.

Variable state:

number of individuals n

$n^j = $ juveniles, $n^a = $ adults, $n = n^j + n^a$

(i) Reproduction

$$n^j = k_c n^a \frac{G - G_{max}}{G_{min}}, \; G^j = G_{min}, \; G^a = G_{max}$$

where reproduction efficiency $k_c = 0.1$ and $G_{min} = 0.2 \; \mu g \; C$.

1071

(ii) Mortality

Mortality after reproduction:

$$\frac{\partial n^a}{\partial t} = \frac{n^a}{-t_w + \int_{t_r}^{t} \mathrm{d}t}, \qquad \text{for } \int \mathrm{d}t \leq t_w - 1^h$$

$t_w = 20$ days

Predation:

$$\frac{\partial n}{\partial t} = -n G_{\text{eff}}^{0.7} k_{pr} \frac{B}{B + k_B} I(z)$$

$k_{pr} = 0.6 \times 10^{-4}$ day^{-1}
B = total zooplankton biomass
$k_B = 12\,000$ μg C m^{-2}

Remineralization

Detritus, faecal pellets and the dead animals are bundled into a number of separate particles. The biomass of the particles decays due to the action of bacteria, following a simple 'radioactive decay' law.

$$\frac{\partial A}{\partial t} = -\frac{\partial C}{\partial t} = aC$$

C is the biomass of the dead material and $a = 0.01$ day^{-1}.
Other ammonium sources are predation, reproduction mortality $0.9n^a(G - G_{\text{max}})$ and the basal zooplankton respiration rate.
   No vertical transfer of nitrate from below the seasonal boundary layer has been taken into account.
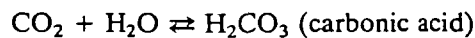
(2) The carbon model

The chemical cycle of CO_2 in the ocean is governed by a series of equilibria:

(i) The CO_2 in the atmosphere equilibrates with seawater via exchange across the air/sea interface
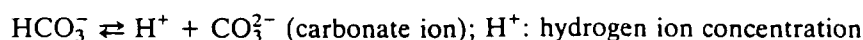
$$CO_2 \text{ (gas)} \rightleftarrows CO_2 \text{ (dissolved)}$$

(ii) The dissolved CO_2 then becomes hydrated

$$CO_2 + H_2O \rightleftarrows H_2CO_3 \text{ (carbonic acid)}$$

1072

(iii) The carbonic acid undergoes very rapid dissociation

$$H_2CO_3 \rightleftharpoons H^+ + HCO_3^- \text{ (bicarbonate ion)}$$

(iv)

$$HCO_3^- \rightleftharpoons H^+ + CO_3^{2-} \text{ (carbonate ion); } H^+: \text{ hydrogen ion concentration}$$

Since the dissociation of carbonic acid to bicarbonate ion is a very fast process, it may for all practical purposes be considered as instantaneous.

The corresponding equilibrium constants can be expressed as follows:

$$K_0 = \frac{[CO_2]}{p}$$

$$K_1 = \frac{[H^+] [HCO_3^-]}{[CO_2]}$$

$$K_2 = \frac{[H^+] [CO_3^{2-}]}{[HCO_3^-]}$$

In addition, two other important reactions that affect the balance of the carbonate chemistry are:

$$K_b = \frac{[H^+] [B(OH)_4^-]}{[B(OH)_3]}$$

$$K_w = [H^+][OH^-]$$

As CO_2 is added to seawater, the total dissolved inorganic carbon

$$TCO_2 = [CO_2] + [HCO_3^-] + [CO_3^{2-}]$$

increases, but the alkalinity

$$A = [HCO_3^-] + 2[CO_3^{2-}] + [B(OH)_4^-] + [OH^-] - [H^+]$$

remains constant.

Photosynthesis and respiration of biological communities change the concentration of dissolved inorganic carbon. Using a constant C/N ratio of 7, the decrease of inorganic carbon can be calculated directly from the phytoplankton uptake of nitrogen. The sources for CO_2 are remineralization and respiration. The surface CO_2 flux is calculated using a constant piston velocity of 4.8 m day^{-1}.

The model calculates the partial pressure of seawater, p, using the method

1073

described by Bacastow and Bjorkstrom (1981), which requires as input: (i) values for the dissociation constants K_0, K_1, K_2, K_b, K_w and (ii) values for TCO_2, boron and alkalinity.

The initial values are:

$B(OH)_3$ = 409 × 10^{-6} mol kg^{-1}

p = 325.03 × 10^{-6} atm., p_{atm} = 345 × 10^{-6} atm.

TCO_2 = 2089.13 × 10^{-6} mol kg^{-1}

A = 2354.61 × 10^{-6} eq kg^{-1}

TCO_2 and alkalinity were calculated using a pH value of 8.25.

The boron concentration, as well as alkalinity, is assumed to remain constant. The dissociation constants are given by Peng *et al.* (1987).

1074